Journal of Aeronautics, Astronautics and Aviation, Vol.49, No.2, pp.083 - 92 (2017)
DOI: 10.6125/17-0109-921

Enhanced GNSS-SAR Range-Doppler Algorithm for The Target Detection of Weak Reflected Signals: An Experimental Study

Yu Zheng [**], Yang Yang and Wu Chen

Department of Land Surveying and Geo-informatics,
The Hong Kong Polytechnic University, Hong Kong, China.

ABSTRACT

A new tool for remote sensing GNSS-SAR is developing recently. However, due to the limitation of narrow signal band of GNSS signals, images generated by GNSS-SAR are much noisy and with low azimuth resolution, particularly when reflected GNSS signals are weak. Due to the issue, a new algorithm is proposed for target detection based on the Range-Doppler algorithm in this paper. Firstly, according to the analysis of the average SNR (signal-to-noise ratio) of the received reflected signal, optimal threshold and range correlation duration are derived for detecting range compressed signal. Thereafter by properly scaling the detected range compressed signals along azimuth domain, we can further enhance the SNR along specified azimuth direction. Thus, when conducting azimuth processing, the azimuth resolution can be improved. In the paper, the new algorithms will be described and the experiment results will be presented.

Keywords: Range-Doppler Algorithm; GNSS-SAR imaging; Signal to noise ratio; Azimuth resolution

I. INTRODUCTION

A new tool known as GNSS-SAR [1, 2], which is a passive SAR receiver that utilizes signals from Global Navigation Satellite Systems (GNSS) i.e. GPS, GLONASS, Galileo or Beidou as source of opportunity, is a developing technique for remote sensing in recent years. Compared with the traditional SAR, GNSS-SAR has the following advantages. 1). Lower cost because there is no necessity in constructing signal trans- mission equipment. 2). Due to the receiver is in the passive mode, it is more flexible for the applications under different environments.

Concerning SAR imaging, because range Doppler method is commonly used, thus many researchers have developed and demonstrated a GNSS-SAR imaging algorithm based on that method correspondingly. According to the literature [1, 2, 7, 8, 9, 11, 12, 13], the main ideal of GNSS-SAR range Doppler algorithm is based on the two separated compressions (i.e. range compression and azimuth compression), in which the detail steps of the algorithm are concluded in [1, 2, 13]. To verify the algorithm, several typical simulations and field experiments have been accomplished in recent years, which are specifically reviewed as follows. In [7], a fixed receiver experiment with multi GPS satellites was carried out on BAO tower under GNSS-SAR range-Doppler algorithm. Meanwhile in the literature [8], the simulation scenario is considered with bi-static SAR under the two cases as fixed GNSS transmitter with moving receiver and non-fixed GNSS transmitter with stationary receiver. Moreover, in order to further verify the effectiveness of GNSS range-Doppler algorithm in bi-SAR system, the literature [9, 11, 12] provide their field experimental results correspondingly under various configuration types.

Based on the works, it can be seen that the feasibility of GNSS-SAR range Doppler algorithm has been demonstrated. However, comparing with traditional SAR chirp signal, because GNSS signals have narrower bandwidth, it is less noise immunity [18, 19]. Particularly

[*] Manuscript received, December 19, 2016, final revision, January 19, 2017, from ISGNSS.
[**] To whom correspondence should be addressed, E-mail: yuzheng175@gmail.com

when reflected signal power is not feasible, for instance no larger than -20 dB, the conventional GNSS-SAR range Doppler algorithm will result in a much noisier image. To our best knowledge, few GNSS-SAR related works have specifically discussed and analyzed the method for dealing with the problem imaging of weak reflected signal. As stated in the literature [10] that for GNSS-SAR imaging, range compression is identically auto-correlation of PRN code, the compression length is limited by one code period, thus the conventionally used method for coping with weak GNSS signal acquisition that to increase coherent correlation duration for several mini-second [3, 4, 5, 14, 15] may not always be applicable. Because of this, the approach that to lengthen azimuth matched filter for suppressing the remaining noise will be conventionally used for guaranteeing the illumination level per azimuth resolution cell. However, based on the analysis of point spread function discussed in [2, 16], the approach will increase the azimuth ambiguity.

In this paper, the main objective is to handle the issue GNSS-SAR imaging of weak reflected signals. To obtain the objective, a new algorithm for enhancing target identifiability on GNSS-SAR image, which is denoted as enhanced GNSS- SAR range Doppler algorithm, is proposed. In the proposed algorithm, firstly, based on the average SNR of reflected GNSS signal, optimal threshold and range correlation duration is estimated for range compressed signal detection. Then we can further enhance the primary azimuth SNR by properly scaling the detected range compressed signals along the azimuth domain. Therefore, when carrying out azimuth compression, the azimuth resolution is supposed to be enhanced correspondingly.

The rest of paper is structured as follow. The methodology analysis is provided in section II; Experimental results are illustrated in section III; Final concluding remark and future work are discussed in section IV.

II. METHODOLOGY ANALYSIS

The research is carried out based on a field experiment. GPS C/A code signal is selected as the GNSS signal of opportunity because its receiver has a higher availability. Ground straightly moving receiver is employed. Experiment design and parameter values are provided in subsection II-A. The analysis of the proposed enhanced GNSS-SAR range Doppler algorithm is given in subsection II-B.

A. Experimental Design and Parameter Values

Among our various conducted related experiments, the one ‘parterre reflection’, which images the distributed parterres is selected as a representative example for analyzing. In the selected experiment, weak reflected signals SNR is SNR=-20 dB, which indicates the typical weak reflected signal case. At first, the system model for the research is provided in Figure 1.

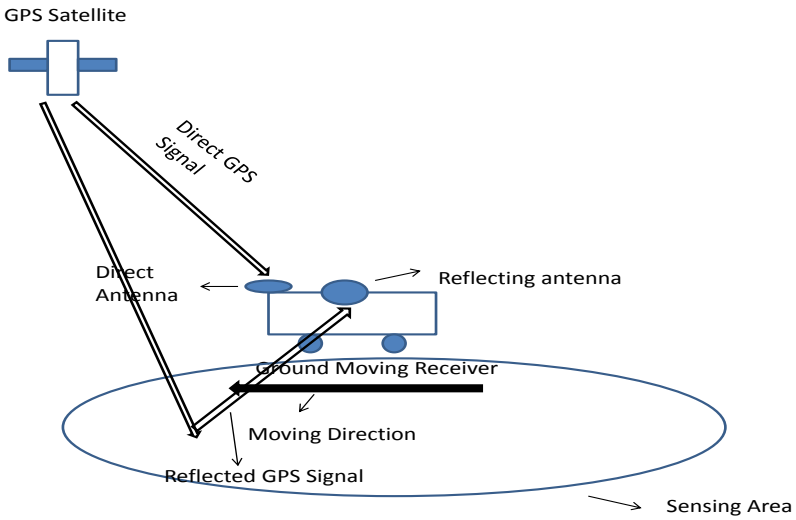

Figure 1 The Implemented System Model

In Figure 1, in order to eliminate direct signal interference at reflected GPS antenna, the source satellite and targeted sensing area should be in the opposite places in horizontal, while the receiver should be located at the place between them.

The field experimental equipment of the GPS C/A code receiver is shown in Figure 2.

In Figure 2(a), direct antenna is of right hand circular polarization type, used for recording direct GPS signal for synchronization. The reflected signal is recorded at reflected antenna, which is left hand circular polarization type1. Both direct and reflected antennas are connected to the same GPS software defined receiver shown in Figure 2(b) and placed on the same moving platform shown in Figure 2(c) for the ease of time synchronization.

(a) (b) (c)

Figure 2 (a) The direct and reflected antenna; (b) The software defined GPS receiver; (c) The straightly ground moving platform

The field experiment denoted as 'parterre reflection', which images four parterres separated only a few meters at imaging azimuth direction of weak reflected signal, is carried out at 6th floor terrace garden, The Hong Kong Polytechnic University. The optical image is presented in Figure 3.

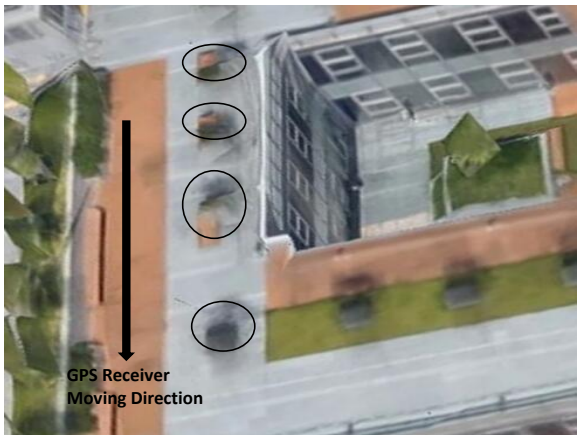

Figure 3 Optical image of parterre reflection experiment [23].

Remark: Because GNSS-SAR has a much superior azimuth resolution than range resolution, for imaging, the parterres are separated at the direction parallel to the receiver moving direction (imaging azimuth direction), but with the same range position.

Aperture synthesizing is conducted at first, which is based on the moving direction illustrated in Figure 3 with 3 minutes duration and a velocity 0.17 m/s, where the satellite movement can be considered as stationary on the earth surface. From a field measurement, along the moving direction, the distance value among the first three parterres is 2 m, while the distance between the third and fourth parterre is 4m. The azimuthal occupation of each parterre is 44 centimeters.

The rest of the parameter values this research is shown in the TABLE 1.

The satellite GPS PRN 21 is selected as transmission of opportunity because it satisfies the geometric position for eliminating direct signal interference at reflected antenna. Number of samples per code period is determined by GPS receiver manufacturer. Azimuth sample quantity is decided by the length of aperture synthesizing, in which the minimum unit of azimuth sample, in which each sample is represented by 1 mini-second.

[1]Reflected signal is much weaker than direct signal, and the left hand circular polarization type has a higher initial sensitivity than right hand circular polarization type. Thus left hand circular polarization type antenna is used as reflected antenna.

Table 1 PARMATER VALUES FOR THE RESEARCH

Parameters	**Values**
Utilized satellite	GPS PRN 21
Transmitting frequency	1575.42 MHz (L1 band)
Utilized PRN code	C/A code
Signal bandwidth	1.023 MHz
Code period	1 ms
Sampling frequency at GPS receiver	1.6368×10 Hz
Number of samples per code period	16368
Number of azimuth samples each range bin	180000

During aperture synthesizing procedure, the received direct GPS signal is expressed as follows.

$$s_d(t,u) = A_d(t,u)C[t-\tau(u)]D[t-\tau(u)] \times \exp(j(\omega_d(u)t+\varphi_d(u)+\varepsilon(u))) + n_d(t,u) \quad (1)$$

where $A_d(\cdot)$ represents the received signal amplitude; $C(\cdot)$ represents PRN code; $D(\cdot)$ represents navigation message; u denotes as azimuth domain, which the upper limited by the duration of aperture synthesizing with 180000 samples; t denotes as range domain, which the upper limited by one PRN code period with 16368 samples; $\tau(\cdot)$ denotes range delay at each azimuth position; and $\omega_d(\cdot)$, $\varphi_d(\cdot)$ denotes Doppler frequency and carrier phase of the receiver at each azimuth position respectively; $\varepsilon(\cdot)$ denotes the caused carrier phase error caused by background environment. These parameters approximately keep unchanged within one code period.

For signal recorded by reflected channel each single reflection point, it can be expressed as

$$s_R(t,u) = A_R(t,u)C[t-\tau(u)-\tau_1(u)] \times D[t-\tau(u)-\tau_1(u)] \times \exp(j(\omega_r(u)t+\varphi_r(u)+\varepsilon(u))) + n_r(t,u) \quad (2)$$

where τ_1 denotes the reflection delay of current point; ωr and φr represent$_1$ the reflected Doppler frequency and carrier phase respectively, which difference between ωd and φd indicates the receiver's displacement. Due to both channels are connected to straightly ground moving receiver, they should have the approximated same error $\varepsilon(\cdot)$, which can be cancelled during range compression stage. At GPS software defined receiver, s_R is saved into 16,368 samples at range domain and 180,000 samples at azimuth domain as well. The received reflected signal of the targeted sensing area is a combination of each single reflection point with different signal amplitude Ar and delayed values τ^l, which expressed as follow.

$$s_r(t,u) = \sum_{l=1}^{L} s_R^l(t-\tau(u)-\tau_1^l(u),u) \quad (3)$$

where l denotes number of reflection points in the imaging area.

After performing aperture synthesizing, direct signal synchronization for constructing imaging matched filter is carried out. The corresponding steps identically follow GPS signal acquisition and tracking procedure, which methodology is already very mutual, thus the related description is omitted at here. The constructed imaging matched filter after performing synchronization is expressed as follow.

$$s_{dM}(t,u) = A_d(t,u)\cdot C[t-\tau(u)]\cdot D[t-\tau(u)] \times \exp(j(\omega_d(u)\cdot t+\varphi_d(u)+\varepsilon(u))) \quad (4)$$

[2]The direct GNSS signals quality depends on the distance between satellite and receiver, which determined by the elevation angle; for reflected GNSS signals, apart from the elevation angle, another important factor objects reflection capability will mainly determine the signal quality.

Imaging procedure by the proposed enhanced GNSS-SAR range Doppler algorithm is carried out followed by, which will be analyzed in detail in the subsection II-B.

B. Enhanced GNSS-SAR Range Doppler Algorithm

The proposing of the enhanced GNSS-SAR range Doppler algorithm is because that the conventional GNSS-SAR range Doppler algorithm may not be capable enough to handle the scenario of weak reflected signal. This will be analyzed at first before introducing the proposed algorithm. The procedure of conventional GNSS-SAR range Doppler algorithm can be seen in the literature [1, 2, 13], where range compressed results each azimuth bin, azimuth compressed result each targeted scene and the result indicating final image are expressed mathematically in the following respectively.

$$T(N_s-1,u) = \frac{1}{N_s}\sum_{k=0}^{N_s-1} s_{dM}(k,u)s_r^*(k,u) \quad (5)$$

$$I_{mi}(N_s-1,M_s-1) = \frac{1}{M_s}\sum_{k_2=0}^{M_s-1} T(N_s-1,k_2)T^*(N_s-1,k_2) \quad (6)$$

$$I_m = \sum_{i=0}^{I-1} I_{mi} \quad (7)$$

where $*$ represents conjugate; k denotes the number of range sample and *Ns* denotes total range sample quantity used for correlation; i denotes the number of targeted azimuth scene; k_2 denotes the number of azimuth samples; Ms denotes the total azimuth sample quantity selected for azimuth sliding correlation, also represents azimuth matched filter length for single resolution cell; *I* denotes the total targeted azimuth resolution cell quantity. Imi and Im denote the compressed result single azimuth resolution cell and final GNSS-SAR image respectively.

Based on the results in the literature [20], it can be seen that to achieve an accepted image quality, SNR should be at least 40 dB. Denote γ as the received reflected SNR; γc is the SNR after performing range correlation for compression; *B* as the GPS signal

bandwidth of the value 1.023 MHz and τR as the correlation duration, which limited by 1 ms, their relationship can be expressed as follows [6].

$$\gamma_c = \gamma \cdot B \cdot \tau_R \quad (8)$$

It can be seen that based on (8), due to the objects reflection capability2, when reflected SNR is as low as no higher than $\gamma = -20$ dB, the best γc can merely reach at the level 10 dB by using the whole PRN code period length for performing range correlation. Concerning azimuth compression of single resolution cell, a similar relationship as (8) can be obtained. Therefore, when $\gamma = -20$ dB, apart from the required azimuth samples to reveal the receiver's displacement obviously, azimuth matched filter should be lengthened to suppress the remaining noise as well to make the illumination level per azimuth resolution cell live up to at least 40 dB level. However, based on the ambiguity function analysis shown in [2, 16], lengthened azimuth matched filter will cause a higher azimuth ambiguity.

Based on the analysis above this subsection, an enhanced GNSS-SAR range Doppler algorithm is proposed, which procedures are illustrated and analyzed as follows[3]

1). Before imaging, threshold and correlation duration is estimated for range compressed signal detection based on the received reflected SNR, stand deviation formed binary hypothesis problem based on the to be conducted range compression each azimuth bin. The trade-off between detection probability and posterior detection rate based on Bayesian rule [21] is used for the threshold and range correlation duration value selection, which is given following

$$\max_{\xi,\tau_R} \rho = \frac{P(H_1)\cdot P_d(\xi,\tau_R f_s)}{P(H_1)\cdot P_d(\xi,\tau_R f_s)+P(H_0)\cdot P_f(\xi,\tau_R f_s)} \quad (9)$$
$$\text{s.t.} \quad P_d(\xi,\tau_R f_s) \geq 0.9$$

where ξ denotes detection threshold; *fs* denotes sampling frequency; $P_d(\cdot)$ and $P_f(.)$ denote detection and false alarm probability respectively; $P(H_0)$ and $P(H_1)$ denote the probability of presence and absence of signal respectively, according to [22], their values are similar for many circumstance. Concerning a decent detection performance, $P_d(\cdot)$ is expected to be larger than 0.9. According to (9) and field study scenario this paper, from simulation, the proper normalized threshold ξ value is determined as 0.7, while 11,200 out of 16,369 range samples are used for range correlation as the compression.

2). Range correlation for compression each azimuth bin with 11,200 range samples.

3). Detecting range compressed signal each azimuth bin according to the normalized threshold value 0.7.

4). Scaling the detected range compressed signal at each azimuth bin for enhancing SNR of azimuth primary signal. Initial scaling factor A should make the illumination level of detected range compressed signal higher than the method using whole code period's correlation; otherwise the proposed algorithm will have no meaning. Based on the research scenario, we can have

$$A > \frac{1\,\text{ms}}{\tau_R} = \frac{16369}{11200} \approx 1.46 \quad (10)$$

To refine the *A* value, it should make the detected least strength signal, which is exactly the threshold level signal strength, reach the required SNR level 40 dB for generating the image of minimum accepted quality the single targeted scene. Through test under the scenario in this paper, *A* is refined to 40dB.

5). Selecting azimuth matched filter based on the scaled detected range compressed signal along azimuth domain with specific length for each scene. Because primary azimuth SNR has already been enhanced to generate decent image quality with regardless of azimuth matched filter length, the chosen the azimuth samples for correlation in compression single scene only needs to be based on observing Doppler frequency changes indicating receiver's displacement obviously. Still based on the analysis of ambiguity function shown in [2, 16], we can have that the azimuth ambiguity the proposed algorithm will be reduced. According to simulation, the length of azimuth matched filter in this algorithm each scene is determined as 6,400 out of 180,000.

6). Azimuth sliding correlation for single scene compression based on the matched filter of the length referred in step 5 and primary azimuth signal, which is scaled detected range compressed signal along azimuth direction.

7). Accumulating the result each scene along azimuth direction.

8). Obtaining final GPS-SAR image.

[3]In this paper, since GNSS satellite is considered as relatively stationary, elevation angle is not the key factor which impacts the performance of the proposed algorithm. Thus, the corresponding discussion is omitted.

III. EXPERIMENTAL RESULTS

In this section, we provide GPS-SAR image generated by the proposed algorithm, the conventional GNSS-SAR range Doppler algorithm as well as the GNSS-SAR range Doppler algorithm with lengthened matched filter at both range domain and azimuth domain. For the algorithm with the lengthened matched filters, the correlation duration is determined as 1 ms at range domain while 23,680 azimuth samples for azimuth correlation each resolution cell. To speed up imaging processing among the to be conducted comparisons, azimuth down sampling by 80 samples is performed before carrying out imaging. This is because the velocity of receiver is slow, the caused Doppler and carrier phase

for azimuth compression can be considered as no changed duration a short azimuth duration, while the value 80 is obtained from numerical simulations. The results are illustrated in Figure 4,correspondingly.

Since the targets are imaged at the same range position, we specifically consider the estimation of azimuth position of Figure 4. As can be seen in Figure 4(a), along aperture synthetic direction, through computation on MATLAB, the number of azimuth samples between first and second, second and third bright scenes are 141; between the second and the third scene is 282. Because originally, each azimuth sample represents 1ms, and azimuth down-sampling by 80 is performed based on the original azimuth domain, 141 samples corresponds to 11.20s and 282 samples corresponds to 22.56 s. Combining the factor that moving velocity is 0.17 m/s, the corresponding distances on Figure 4 (a) can be calculated as 0.17 m/s×11.20 s = 1.90 m and 0.17 m/s × 22.56 s = 3.84 m respectively, which can match with the distances are 2 m and 4 m according to field measurement results in general. In Figure 4(b), due to the fact that based on the conventional GNSS-SAR range Doppler algorithm, range compressed signals have not been correctly detected and scaled to an expected decibel level along azimuth domain, and also the matched filters length at both range and azimuth domain cannot capability suppress noise, the obtained GPS-SAR image is quite noisy with the illumination level of the degree 102 less than Figure 4(a).

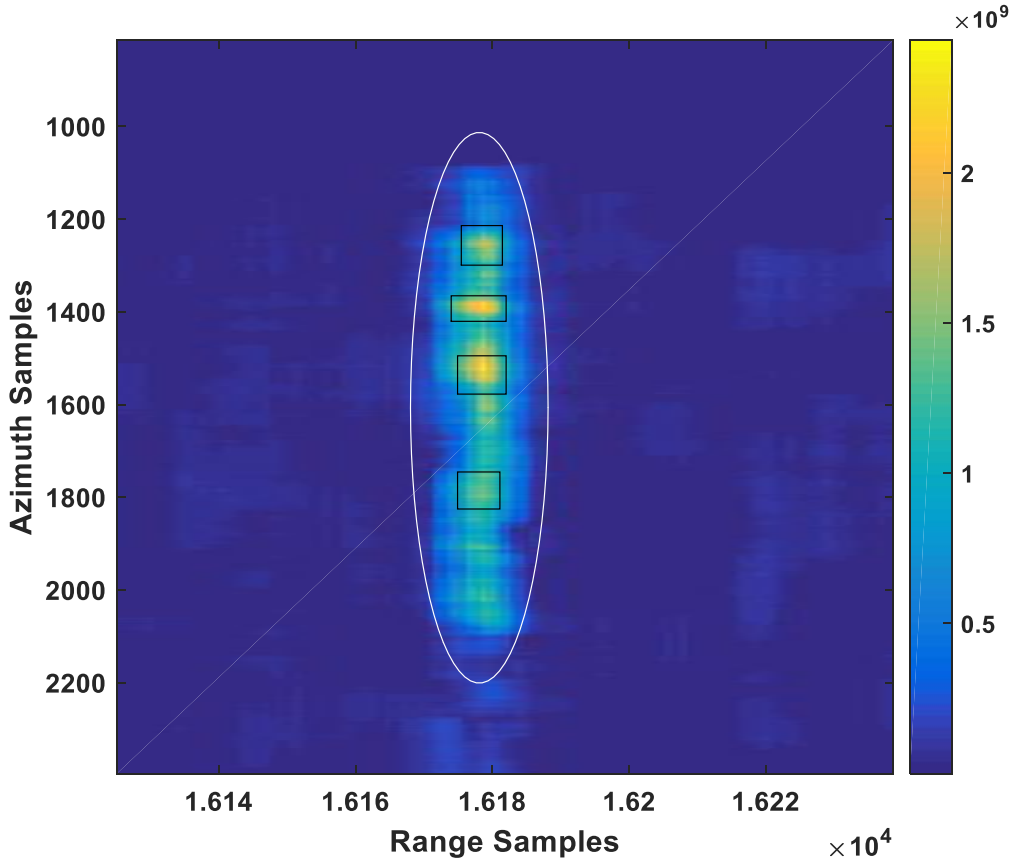

Figure 4 (a) The GPS-SAR image generated by the proposed algorithm;

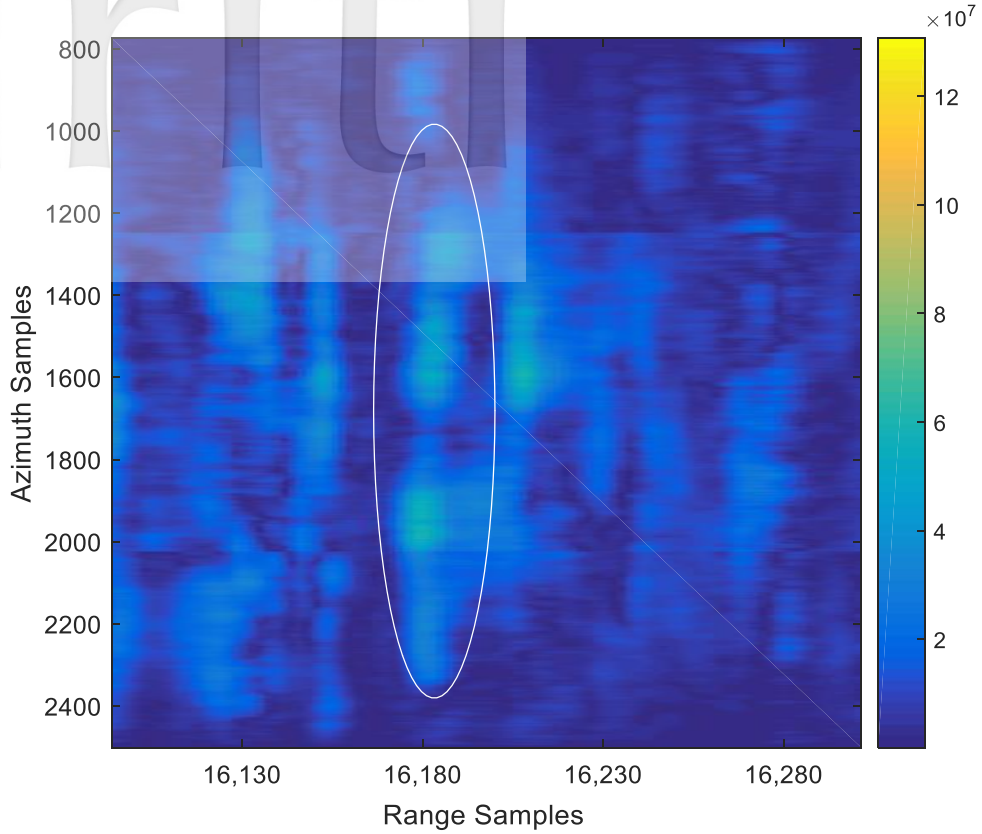

Figure 4 (b) The GPS-SAR image generated by conventional range Doppler algorithm;

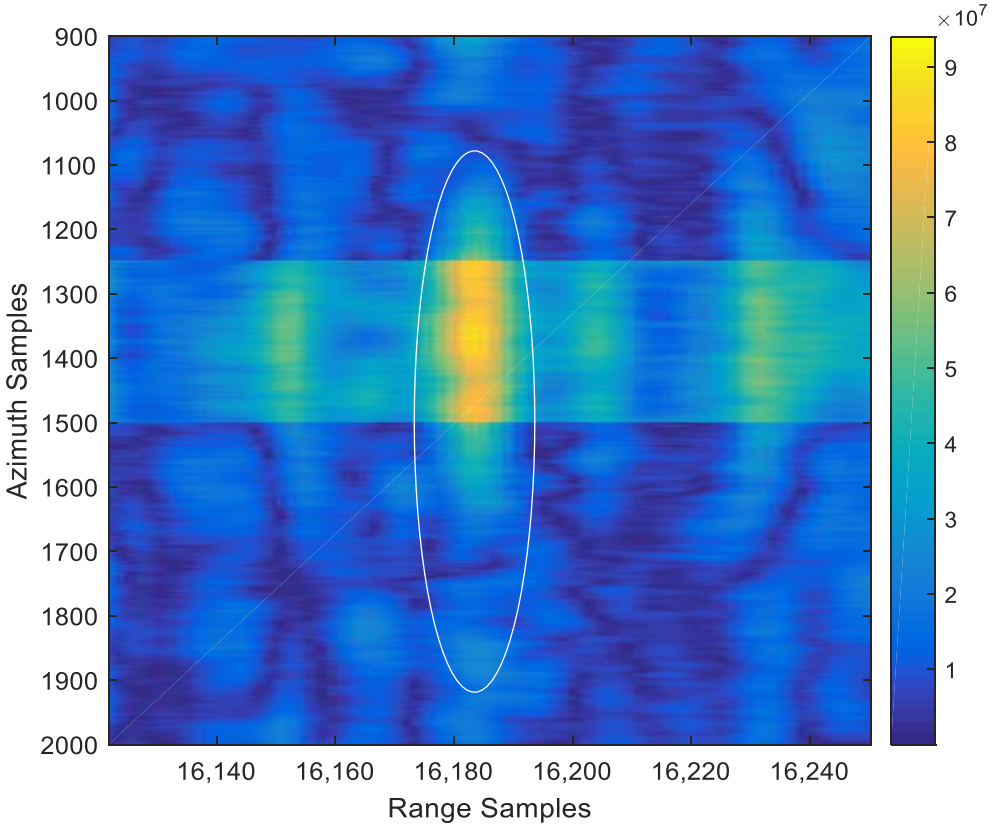

Figure 4 (c) The GPS-SAR image generated by the range Doppler algorithm with lengthened range and azimuth matched filter.

Table 2 MACHINE RUNNING TIME THROUGHOUT RANGE COMPRESSION PROCESSING

The proposed algorithm	Conventional GNSS-SAR range Doppler algorithm	**The GNSS-SAR Range Doppler algorithm with the lengthened range and azimuth matched filter**
15.012s	15.012s	47.538s

Therefore, it is difficult to identify the targets four distributed parterres on Figure 4(b). Concerning Figure 4(c), because that matched filters are lengthened at both range and azimuth domain, the illumination level is enhanced of the degree 4 times higher than Figure 4(b) according to the measurement on MATLAB platform. However due to the lengthened matched filters, compared with Figure 4(a), the azimuthal ambiguity is obviously increased at the same time. Concerning range computational burden, the comparison results among Figure 4(a) to Figure 4(c) are given in Table 2.

Based on both Table 2 and Figure 4, we can see that the proposed algorithm for dealing with weak reflected GNSS signal can not only improve scene illumination level and azimuth resolution of GPS-SAR image, but also will not increase the range computational burden.

Thereafter we further study the best attainable azimuth resolution of the generated GPS-SAR image by the proposed algorithm shown in Figure 4(a). Through the computation using MATLAB, the second illuminated scene is of a least azimuthal ambiguity. Thus, we zoom that scene for the ease of illustration. The zoomed image is shown in Figure 5.

As can be seen in Figure 5, the lower azimuthal bound of this bright scene is 1,377 samples, while the upper azimuthal bound is 1,411 samples. Therefore, the azimuthal occupation of the scene is 34. Because azimuthal down-sampling by 80 is employed, 34 samples corresponds to 2.72 s. Due to the fact that motion speed is 0.17 m/s, the azimuthal occupation of the illuminated scene is 43.5 cm, which generally matches with the field measured value 44 cm. In summary, the best azimuthal resolution can be obtained at a level less than 1 meter.

Furthermore, through tests, the proposed algorithm is applicable for the remote sensing scenario of other topological models of weak reflected signals with other GNSS satellites as source of opportunities as well. However due to the fact that the exact reflected SNR of the weak signal will not always be the same as this paper, based on the criterion (9), the exact values of threshold and range correlation length determination for detecting range compressed signal per azimuth bin will be different as well.

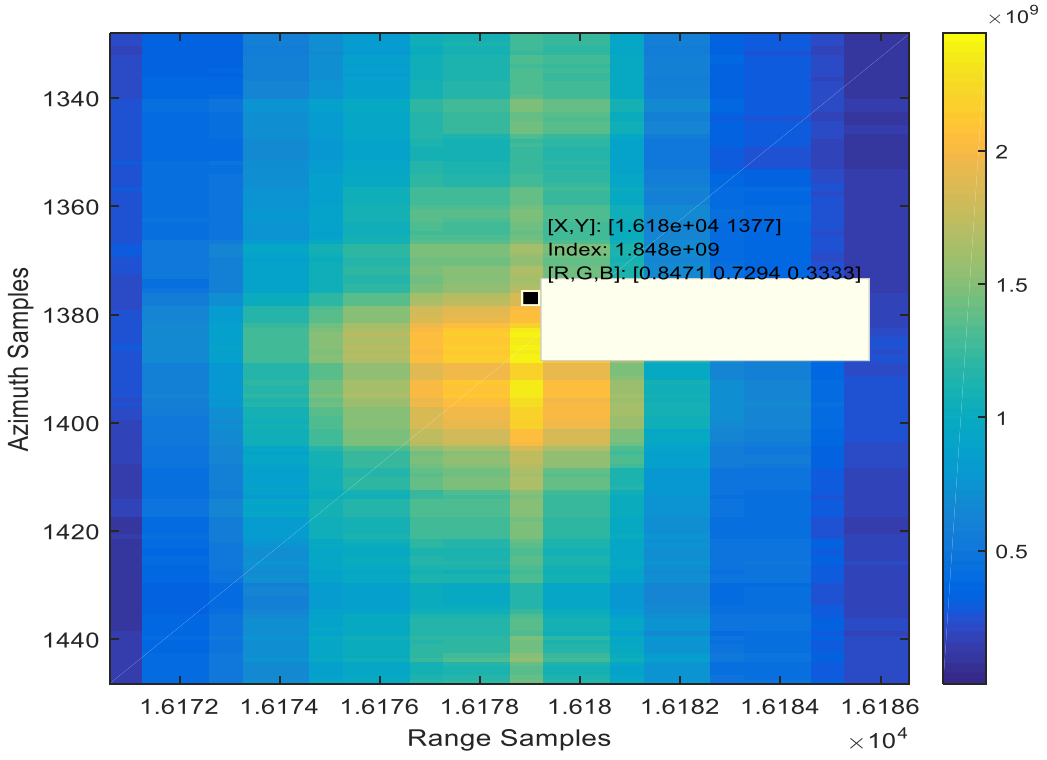

(a)

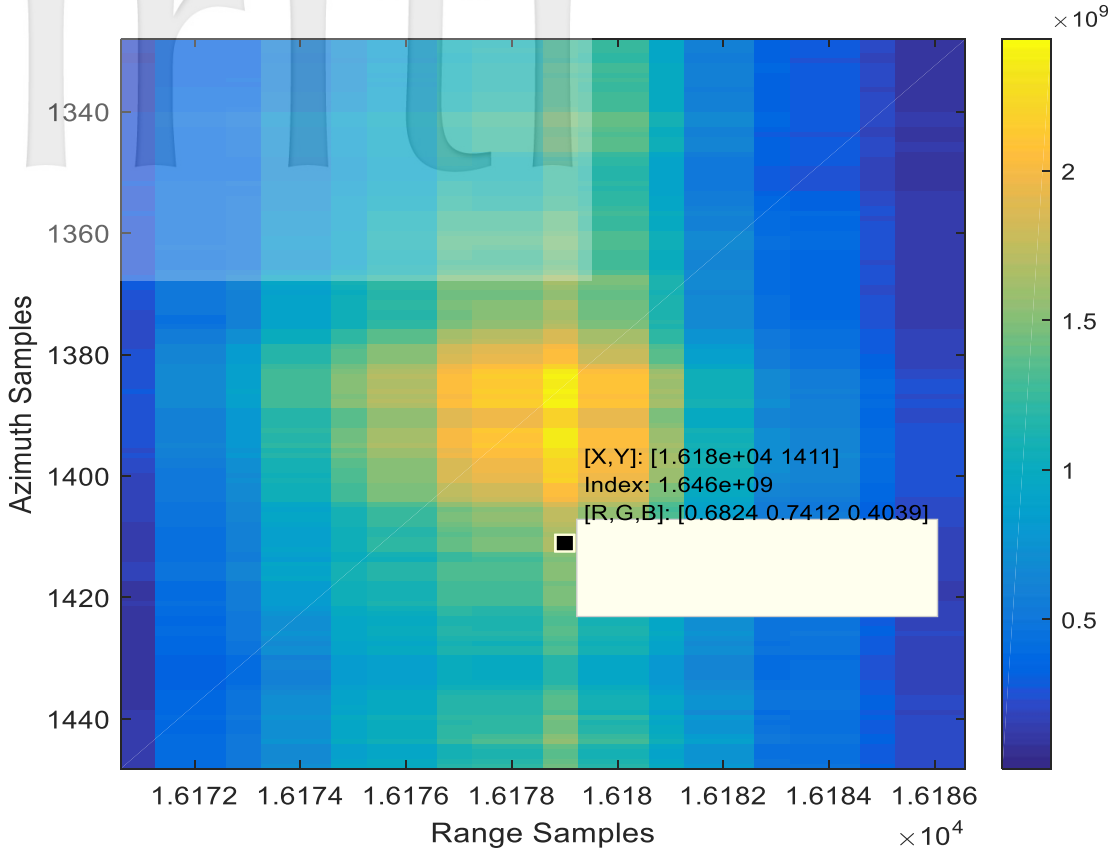

(b)

Figure 5 The zoomed image of the second bright scene in Figure 4(a)

IV. CONCLUSIONS AND FUTURE WORK

GNSS-SAR imaging of weak reflected signal is addressed in this paper. Because particularly when reflected signal power is weak, the generated image will become noisy and with a low azimuth resolution by using the conventional GNSS- SAR range Doppler algorithm, an enhanced GNSS-SAR range Doppler algorithm is proposed for handling the problem. Concerning the proposed algorithm, proper threshold and range correlation time are determined for detecting range compressed signal based on the estimation of the reflected SNR. Then after performing range compression, the detected range compressed signal is scaled along azimuth domain, where primary azimuth SNR is enhanced. Therefore, azimuth resolution can be improved correspondingly when carrying out azimuth compression. The research is conducted based on a filed experiment. The experimental results reveal that for coping with weak reflected signal issue, the proposed algorithm can provide enhanced illumination level and azimuth resolution than the conventional GNSS-SAR range Doppler algorithm, and will not increase the range computational burden. In addition, the best azimuth resolution the proposed algorithm provides can reach at the level less than 1 meter.

Earthquake is one of the natural hazards which cause many damages. And because of the damages, the reflection properties of a certain region will be different before and after earthquake happens. Therefore, it would be possible that to study the level of earth quake damages based on the illuminated parts of the corresponding GNSS-SAR images. In our future work, we would like to apply GNSS-SAR technique in earthquake damage monitoring, and developing the related schemes to improve the monitoring accuracy.

ACKNOWLEDGMENT

The research was substantially by funded by Hong Kong Research Grants Council (RGC) Competitive Earmarked Re- search Grant (Project No: 15202314), Hong Kong Innovation and Technology Fund (ITP/042/13LP) and the research fund from the Research Institute of Sustainable Urban Development, Hong Kong Polytechnic University.

REFERENCES

[1] Zuo, R., “Bistatic synthetic aperture radar using GNSS as transmitters of opportunity”, PhD Thesis, University of Birmingham, 2012.

[2] Zeng, Z., “Passive bistatic SAR with GNSS transmitter and a stationary receiver”, PhD Thesis, University of Birmingham, 2013.

[3] Kaplan, E., and Hegarty, C., editors, "*Understanding GPS: principles and applications*", Artech house, 2005.
[4] Ziedan, N. I., "*GNSS receivers for weak signals*", Energy, Vol. 1992, 2006.
[5] Borre, K., Akos, D. M. , Bertelsen, N., Rinder, P., and Jensen, S. H., "*A Software-Defined GPS and Galileo receiver: a single-frequency approach*", Springer Science & Business Media, 2007.
[6] Malanowski, M., and Kulpa, K., "Analysis of integration gain in passive radar", *IEEE International Conference on Radar*, pp. 323–328, 2008.
[7] Lindgren, T. and Akos, D. M., "A multistatic GNSS synthetic aperture radar for surface characterization", *IEEE Transactions on Geoscience and Remote Sensing*, Vol. 46, No. 8, pp. 2249–2253, 2008.
[8] Antoniou, M., Cherniakov, M., and Hu, C., "Space-surface bistatic SAR image formation algorithms", *IEEE Transactions on Geoscience and Remote Sensing*, Vol. 47, No. 6, pp. 1827–1843, 2009.
[9] Antoniou, M., Zeng, Z., Feifeng, L., and Cherniakov, M., "Experimental demonstration of passive BSAR imaging using navigation satellites and a fixed receiver", *IEEE Geoscience and Remote Sensing Letters*, Vol. 9, No. 3, pp. 477–481, 2012.
[10] Mikawa, Y., Ebinuma, T., and Nakasuka, S., "The study of the remote- sensing application using the GNSS reflected signal with the aperture synthesis", *IEEE International In Geoscience and Remote Sensing Symposium (IGARSS)*, pp. 400–403, 2012.
[11] Antoniou, M., and Cherniakov, M., "Experimental demonstration of passive GNSS-based SAR imaging modes", *2013 IET International Radar Conference*, pp. 1–5, 2013.
[12] Antoniou, M., Hong, Z., Zhangfan, Z., Zuo, R., Zhang, Q., and Cherniakov, M., "Passive bistatic synthetic aperture radar imaging with Galileo transmitters and a moving receiver: experimental demonstration", *IET Radar, Sonar & Navigation*, Vol. 7, No. 9, pp. 985–993, 2013.
[13] Antoniou, M. and Cherniakov, M., "GNSS-based bistatic SAR: a signal processing view", *EURASIP Journal on Advances in Signal Processing*, 2013(1), pp. 1–16, 2013.
[14] Rao, X., Tao, H., Xie, J., Su, J., and Li, W., "Long-time coherent integration detection of weak maneuvering target via integration algorithm, improved axis rotation discrete chirp-Fourier transform", *IET Radar, Sonar & Navigation*, Vol. 9, No. 7, pp. 917–926, 2015.
[15] Chen, X., Guan, J., Liu, N., and He, Y., "Maneuvering target detection via Radon-fractional Fourier transform-based long-time coherent integration", *IEEE Transactions on Signal Processing*, Vol. 62, No. 4, pp. 939-953, 2014.
[16] Santi, F., Antoniou, M., and Pastina, D., "Point spread function analysis for GNSS-based multistatic SAR", *IEEE Geoscience and Remote Sensing Letters*, Vol. 12, No. 2, pp. 304–308, 2015.
[17] Turin, G,. "An introduction to matched filters", *IRE transactions on Information theory*, Vol. 3, No. 6, pp. 311–329, 1960.
[18] Springer, A., Gugler, W., Huemer, M., Reind, L., Ruppel, C. C., and Weigel, R., "Spread spectrum communications using chirp signals", *IEEE/AFCEA Information Systems for Enhanced Public Safety and Security*, pp. 166–170, 2000.
[19] Peterson, R. L., Ziemer, R. E. and Borth, D. E., "*Introduction to spread- spectrum communications*", New Jersey: Prentice Hall, April 1995.
[20] Steven, W. S., *The scientist and engineer's guide to digital signal processing*, California Technical Pub, 1997.
[21] Kobayashi, H., Mark, B. L., and Turin, W., *Probability, Random Processes, and Statistical Analysis*, United Kingdom at the University Press, Cambridge, 2012.
[22] Levy, B. C., "Principles of signal detection and parameter estimation", Springer Science & Business Media, July 7, 2008.
[23] http://www.google.cn/maps, available on April 28, 2016.